

# Pion Interferometry in Au+Au and Cu+Cu Collisions at $\sqrt{s_{NN}} = 62.4$ and 200 GeV

B. I. Abelev,<sup>8</sup> M. M. Aggarwal,<sup>30</sup> Z. Ahammed,<sup>47</sup> B. D. Anderson,<sup>18</sup> D. Arkhipkin,<sup>12</sup> G. S. Averichev,<sup>11</sup> J. Balewski,<sup>22</sup> O. Barannikova,<sup>8</sup> L. S. Barnby,<sup>2</sup> J. Baudot,<sup>16</sup> S. Baumgart,<sup>52</sup> D. R. Beavis,<sup>3</sup> R. Bellwied,<sup>50</sup> F. Benedosso,<sup>27</sup> M. J. Betancourt,<sup>22</sup> R. R. Betts,<sup>8</sup> A. Bhasin,<sup>17</sup> A. K. Bhati,<sup>30</sup> H. Bichsel,<sup>49</sup> J. Bielcik,<sup>10</sup> J. Bielcikova,<sup>10</sup> B. Biritz,<sup>6</sup> L. C. Bland,<sup>3</sup> M. Bombara,<sup>2</sup> B. E. Bonner,<sup>36</sup> M. Botje,<sup>27</sup> J. Bouchet,<sup>18</sup> E. Braidot,<sup>27</sup> A. V. Brandin,<sup>25</sup> E. Bruna,<sup>52</sup> S. Bueltmann,<sup>29</sup> T. P. Burton,<sup>2</sup> M. Bystersky,<sup>10</sup> X. Z. Cai,<sup>40</sup> H. Caines,<sup>52</sup> M. Calderón de la Barca Sánchez,<sup>5</sup> O. Catu,<sup>52</sup> D. Cebra,<sup>5</sup> R. Cendejas,<sup>6</sup> M. C. Cervantes,<sup>42</sup> Z. Chajecski,<sup>28</sup> P. Chaloupka,<sup>10</sup> S. Chattopadhyay,<sup>47</sup> H. F. Chen,<sup>38</sup> J. H. Chen,<sup>18</sup> J. Y. Chen,<sup>51</sup> J. Cheng,<sup>44</sup> M. Cherney,<sup>9</sup> A. Chikanian,<sup>52</sup> K. E. Choi,<sup>34</sup> W. Christie,<sup>3</sup> R. F. Clarke,<sup>42</sup> M. J. M. Codrington,<sup>42</sup> R. Corliss,<sup>22</sup> T. M. Cormier,<sup>50</sup> M. R. Cosentino,<sup>37</sup> J. G. Cramer,<sup>49</sup> H. J. Crawford,<sup>4</sup> D. Das,<sup>5</sup> S. Dash,<sup>13</sup> M. Daugherty,<sup>43</sup> L. C. De Silva,<sup>50</sup> T. G. Dedovich,<sup>11</sup> M. DePhillips,<sup>3</sup> A. A. Derevschikov,<sup>32</sup> R. Derradi de Souza,<sup>7</sup> L. Didenko,<sup>3</sup> P. Djawotho,<sup>42</sup> S. M. Dogra,<sup>17</sup> X. Dong,<sup>21</sup> J. L. Drachenberg,<sup>42</sup> J. E. Draper,<sup>5</sup> F. Du,<sup>52</sup> J. C. Dunlop,<sup>3</sup> M. R. Dutta Mazumdar,<sup>47</sup> W. R. Edwards,<sup>21</sup> L. G. Efimov,<sup>11</sup> E. Elhalhuli,<sup>2</sup> M. Elnimr,<sup>50</sup> V. Emelianov,<sup>25</sup> J. Engelage,<sup>4</sup> G. Eppley,<sup>36</sup> B. Erazmus,<sup>41</sup> M. Estienne,<sup>16</sup> L. Eun,<sup>31</sup> P. Fachini,<sup>3</sup> R. Fatemi,<sup>19</sup> J. Fedorisin,<sup>11</sup> A. Feng,<sup>51</sup> P. Filip,<sup>12</sup> E. Finch,<sup>52</sup> V. Fine,<sup>3</sup> Y. Fisyak,<sup>3</sup> C. A. Gagliardi,<sup>42</sup> L. Gaillard,<sup>2</sup> D. R. Gangadharan,<sup>6</sup> M. S. Ganti,<sup>47</sup> E. J. Garcia-Solis,<sup>8</sup> Geromitsos,<sup>41</sup> F. Geurts,<sup>36</sup> V. Ghazikhanian,<sup>6</sup> P. Ghosh,<sup>47</sup> Y. N. Gorbunov,<sup>9</sup> A. Gordon,<sup>3</sup> O. Grebenyuk,<sup>21</sup> D. Grosnick,<sup>46</sup> B. Grube,<sup>34</sup> S. M. Guertin,<sup>6</sup> K. S. F. F. Guimaraes,<sup>37</sup> A. Gupta,<sup>17</sup> N. Gupta,<sup>17</sup> W. Guryn,<sup>3</sup> B. Haag,<sup>5</sup> T. J. Hallman,<sup>3</sup> A. Hamed,<sup>42</sup> J. W. Harris,<sup>52</sup> W. He,<sup>15</sup> M. Heinz,<sup>52</sup> S. Heppelmann,<sup>31</sup> B. Hippolyte,<sup>16</sup> A. Hirsch,<sup>33</sup> E. Hjort,<sup>21</sup> A. M. Hoffman,<sup>22</sup> G. W. Hoffmann,<sup>43</sup> D. J. Hofman,<sup>8</sup> R. S. Hollis,<sup>8</sup> H. Z. Huang,<sup>6</sup> T. J. Humanic,<sup>28</sup> G. Igo,<sup>6</sup> A. Iordanova,<sup>8</sup> P. Jacobs,<sup>21</sup> W. W. Jacobs,<sup>15</sup> P. Jakl,<sup>10</sup> C. Jena,<sup>13</sup> F. Jin,<sup>40</sup> C. L. Jones,<sup>22</sup> P. G. Jones,<sup>2</sup> J. Joseph,<sup>18</sup> E. G. Judd,<sup>4</sup> S. Kabana,<sup>41</sup> K. Kajimoto,<sup>43</sup> K. Kang,<sup>44</sup> J. Kapitan,<sup>10</sup> D. Keane,<sup>18</sup> A. Kechechyan,<sup>11</sup> D. Kettler,<sup>49</sup> V. Yu. Khodyrev,<sup>32</sup> D. P. Kikola,<sup>21</sup> J. Kiryluk,<sup>21</sup> A. Kisiel,<sup>28</sup> S. R. Klein,<sup>21</sup> A. G. Knospe,<sup>52</sup> A. Kocoloski,<sup>22</sup> D. D. Koetke,<sup>46</sup> M. Kopytine,<sup>18</sup> W. Korsch,<sup>19</sup> L. Kotchenda,<sup>25</sup> V. Kouchpil,<sup>10</sup> P. Kravtsov,<sup>25</sup> V. I. Kravtsov,<sup>32</sup> K. Krueger,<sup>1</sup> M. Krus,<sup>10</sup> C. Kuhn,<sup>16</sup> L. Kumar,<sup>30</sup> P. Kurnadi,<sup>6</sup> M. A. C. Lamont,<sup>3</sup> J. M. Landgraf,<sup>3</sup> S. LaPointe,<sup>50</sup> J. Lauret,<sup>3</sup> A. Lebedev,<sup>3</sup> R. Lednicky,<sup>12</sup> C-H. Lee,<sup>34</sup> J. H. Lee,<sup>3</sup> W. Leight,<sup>22</sup> M. J. LeVine,<sup>3</sup> Li,<sup>51</sup> C. Li,<sup>38</sup> Y. Li,<sup>44</sup> G. Lin,<sup>52</sup> S. J. Lindenbaum,<sup>26</sup> M. A. Lisa,<sup>28</sup> F. Liu,<sup>51</sup> J. Liu,<sup>36</sup> L. Liu,<sup>51</sup> T. Ljubicic,<sup>3</sup> W. J. Llope,<sup>36</sup> R. S. Longacre,<sup>3</sup> W. A. Love,<sup>3</sup> Y. Lu,<sup>38</sup> T. Ludlam,<sup>3</sup> G. L. Ma,<sup>40</sup> Y. G. Ma,<sup>40</sup> D. P. Mahapatra,<sup>13</sup> R. Majka,<sup>52</sup> O. I. Mall,<sup>5</sup> L. K. Mangotra,<sup>17</sup> R. Manweiler,<sup>46</sup> S. Margetis,<sup>18</sup> C. Markert,<sup>43</sup> H. S. Matis,<sup>21</sup> Yu. A. Matulenko,<sup>32</sup> T. S. McShane,<sup>9</sup> A. Meschanin,<sup>32</sup> R. Milner,<sup>22</sup> N. G. Minaev,<sup>32</sup> S. Mioduszewski,<sup>42</sup> A. Mischke,<sup>27</sup> J. Mitchell,<sup>36</sup> B. Mohanty,<sup>47</sup> D. A. Morozov,<sup>32</sup> M. G. Munhoz,<sup>37</sup> B. K. Nandi,<sup>14</sup> C. Nattrass,<sup>52</sup> T. K. Nayak,<sup>47</sup> J. M. Nelson,<sup>2</sup> P. K. Netrakanti,<sup>33</sup> M. J. Ng,<sup>4</sup> L. V. Nogach,<sup>32</sup> S. B. Nurushev,<sup>32</sup> G. Odyniec,<sup>21</sup> A. Ogawa,<sup>3</sup> H. Okada,<sup>3</sup> V. Okorokov,<sup>25</sup> D. Olson,<sup>21</sup> M. Pachr,<sup>10</sup> B. S. Page,<sup>15</sup> S. K. Pal,<sup>47</sup> Y. Pandit,<sup>18</sup> Y. Panebratsev,<sup>11</sup> S. Y. Panitkin,<sup>3</sup> T. Pawlak,<sup>48</sup> T. Peitzmann,<sup>27</sup> V. Perevoztchikov,<sup>3</sup> C. Perkins,<sup>4</sup> W. Peryt,<sup>48</sup> S. C. Phatak,<sup>13</sup> M. Planinic,<sup>53</sup> J. Pluta,<sup>48</sup> N. Poljak,<sup>53</sup> A. M. Poskanzer,<sup>21</sup> B. V. K. S. Potukuchi,<sup>17</sup> D. Prindle,<sup>49</sup> C. Pruneau,<sup>50</sup> N. K. Pruthi,<sup>30</sup> J. Putschke,<sup>52</sup> R. Raniwala,<sup>35</sup> S. Raniwala,<sup>35</sup> R. L. Ray,<sup>43</sup> R. Redwine,<sup>22</sup> R. Reed,<sup>5</sup> A. Ridiger,<sup>25</sup> H. G. Ritter,<sup>21</sup> J. B. Roberts,<sup>36</sup> O. V. Rogachevskiy,<sup>11</sup> J. L. Romero,<sup>5</sup> A. Rose,<sup>21</sup> C. Roy,<sup>41</sup> L. Ruan,<sup>3</sup> M. J. Russcher,<sup>27</sup> R. Sahoo,<sup>41</sup> I. Sakrejda,<sup>21</sup> T. Sakuma,<sup>22</sup> S. Salur,<sup>21</sup> J. Sandweiss,<sup>52</sup> M. Sarsour,<sup>42</sup> J. Schambach,<sup>43</sup> R. P. Scharenberg,<sup>33</sup> N. Schmitz,<sup>23</sup> J. Seger,<sup>9</sup> I. Selyuzhenkov,<sup>15</sup> P. Seyboth,<sup>23</sup> A. Shabetai,<sup>16</sup> E. Shahaliev,<sup>11</sup> M. Shao,<sup>38</sup> M. Sharma,<sup>50</sup> S. S. Shi,<sup>51</sup> X-H. Shi,<sup>40</sup> E. P. Sichtermann,<sup>21</sup> F. Simon,<sup>23</sup> R. N. Singaraju,<sup>47</sup> M. J. Skoby,<sup>33</sup> N. Smirnov,<sup>52</sup> R. Snellings,<sup>27</sup> P. Sorensen,<sup>3</sup> J. Sowinski,<sup>15</sup> H. M. Spinka,<sup>1</sup> B. Srivastava,<sup>33</sup> A. Stadnik,<sup>11</sup> T. D. S. Stanislaus,<sup>46</sup> D. Staszak,<sup>6</sup> M. Strikhanov,<sup>25</sup> B. Stringfellow,<sup>33</sup> A. A. P. Suaide,<sup>37</sup> M. C. Suarez,<sup>8</sup> N. L. Subba,<sup>18</sup> M. Sumera,<sup>10</sup> X. M. Sun,<sup>21</sup> Y. Sun,<sup>38</sup> Z. Sun,<sup>20</sup> B. Surrow,<sup>22</sup> T. J. M. Symons,<sup>21</sup> A. Szanto de Toledo,<sup>37</sup> J. Takahashi,<sup>7</sup> A. H. Tang,<sup>3</sup> Z. Tang,<sup>38</sup> T. Tarnowsky,<sup>33</sup> D. Thein,<sup>43</sup> J. H. Thomas,<sup>21</sup> J. Tian,<sup>40</sup> A. R. Timmins,<sup>2</sup> S. Timoshenko,<sup>25</sup> D. Tlusty,<sup>10</sup> M. Tokarev,<sup>11</sup> T. A. Trainor,<sup>49</sup> V. N. Tram,<sup>21</sup> A. L. Trattner,<sup>4</sup> S. Trentalange,<sup>6</sup> R. E. Tribble,<sup>42</sup> O. D. Tsai,<sup>6</sup> J. Ulery,<sup>33</sup> T. Ullrich,<sup>3</sup> D. G. Underwood,<sup>1</sup> G. Van Buren,<sup>3</sup> M. van Leeuwen,<sup>27</sup> A. M. Vander Molen,<sup>24</sup> J. A. Vanfossen, Jr.,<sup>18</sup> R. Varma,<sup>14</sup> G. M. S. Vasconcelos,<sup>7</sup> I. M. Vasilevski,<sup>12</sup> A. N. Vasiliev,<sup>32</sup> F. Videbaek,<sup>3</sup> S. E. Vigdor,<sup>15</sup> Y. P. Viyogi,<sup>13</sup> S. Vokal,<sup>11</sup> S. A. Voloshin,<sup>50</sup> M. Wada,<sup>43</sup> W. T. Waggoner,<sup>9</sup> M. Walker,<sup>22</sup> F. Wang,<sup>33</sup> G. Wang,<sup>6</sup> J. S. Wang,<sup>20</sup> Q. Wang,<sup>33</sup> X. Wang,<sup>44</sup> X. L. Wang,<sup>38</sup> Y. Wang,<sup>44</sup> G. Webb,<sup>19</sup> J. C. Webb,<sup>46</sup> G. D. Westfall,<sup>24</sup> C. Whitten Jr.,<sup>6</sup> H. Wieman,<sup>21</sup> S. W. Wissink,<sup>15</sup> R. Witt,<sup>45</sup> Y. Wu,<sup>51</sup> W. Xie,<sup>33</sup> N. Xu,<sup>21</sup> Q. H. Xu,<sup>39</sup> Y. Xu,<sup>38</sup> Z. Xu,<sup>3</sup> Yang,<sup>20</sup> P. Yepes,<sup>36</sup> I-K. Yoo,<sup>34</sup> Q. Yue,<sup>44</sup> M. Zawisza,<sup>48</sup> H. Zbroszczyk,<sup>48</sup> W. Zhan,<sup>20</sup> S. Zhang,<sup>40</sup> W. M. Zhang,<sup>18</sup> X. P. Zhang,<sup>21</sup> Y. Zhang,<sup>21</sup> Z. P. Zhang,<sup>38</sup> Y. Zhao,<sup>38</sup> C. Zhong,<sup>40</sup> J. Zhou,<sup>36</sup> R. Zoulkarneev,<sup>12</sup> Y. Zoulkarneeva,<sup>12</sup> and J. X. Zuo<sup>40</sup>

## (STAR Collaboration)

- <sup>1</sup>Argonne National Laboratory, Argonne, Illinois 60439, USA  
<sup>2</sup>University of Birmingham, Birmingham, United Kingdom  
<sup>3</sup>Brookhaven National Laboratory, Upton, New York 11973, USA  
<sup>4</sup>University of California, Berkeley, California 94720, USA  
<sup>5</sup>University of California, Davis, California 95616, USA  
<sup>6</sup>University of California, Los Angeles, California 90095, USA  
<sup>7</sup>Universidade Estadual de Campinas, Sao Paulo, Brazil  
<sup>8</sup>University of Illinois at Chicago, Chicago, Illinois 60607, USA  
<sup>9</sup>Creighton University, Omaha, Nebraska 68178, USA  
<sup>10</sup>Nuclear Physics Institute AS CR, 250 68 Řež/Prague, Czech Republic  
<sup>11</sup>Laboratory for High Energy (JINR), Dubna, Russia  
<sup>12</sup>Particle Physics Laboratory (JINR), Dubna, Russia  
<sup>13</sup>Institute of Physics, Bhubaneswar 751005, India  
<sup>14</sup>Indian Institute of Technology, Mumbai, India  
<sup>15</sup>Indiana University, Bloomington, Indiana 47408, USA  
<sup>16</sup>Institut de Recherches Subatomiques, Strasbourg, France  
<sup>17</sup>University of Jammu, Jammu 180001, India  
<sup>18</sup>Kent State University, Kent, Ohio 44242, USA  
<sup>19</sup>University of Kentucky, Lexington, Kentucky, 40506-0055, USA  
<sup>20</sup>Institute of Modern Physics, Lanzhou, China  
<sup>21</sup>Lawrence Berkeley National Laboratory, Berkeley, California 94720, USA  
<sup>22</sup>Massachusetts Institute of Technology, Cambridge, MA 02139-4307, USA  
<sup>23</sup>Max-Planck-Institut für Physik, Munich, Germany  
<sup>24</sup>Michigan State University, East Lansing, Michigan 48824, USA  
<sup>25</sup>Moscow Engineering Physics Institute, Moscow Russia  
<sup>26</sup>City College of New York, New York City, New York 10031, USA  
<sup>27</sup>NIKHEF and Utrecht University, Amsterdam, The Netherlands  
<sup>28</sup>Ohio State University, Columbus, Ohio 43210, USA  
<sup>29</sup>Old Dominion University, Norfolk, VA, 23529, USA  
<sup>30</sup>Panjab University, Chandigarh 160014, India  
<sup>31</sup>Pennsylvania State University, University Park, Pennsylvania 16802, USA  
<sup>32</sup>Institute of High Energy Physics, Protvino, Russia  
<sup>33</sup>Purdue University, West Lafayette, Indiana 47907, USA  
<sup>34</sup>Pusan National University, Pusan, Republic of Korea  
<sup>35</sup>University of Rajasthan, Jaipur 302004, India  
<sup>36</sup>Rice University, Houston, Texas 77251, USA  
<sup>37</sup>Universidade de Sao Paulo, Sao Paulo, Brazil  
<sup>38</sup>University of Science & Technology of China, Hefei 230026, China  
<sup>39</sup>Shandong University, Jinan, Shandong 250100, China  
<sup>40</sup>Shanghai Institute of Applied Physics, Shanghai 201800, China  
<sup>41</sup>SUBATECH, Nantes, France  
<sup>42</sup>Texas A&M University, College Station, Texas 77843, USA  
<sup>43</sup>University of Texas, Austin, Texas 78712, USA  
<sup>44</sup>Tsinghua University, Beijing 100084, China  
<sup>45</sup>United States Naval Academy, Annapolis, MD 21402, USA  
<sup>46</sup>Valparaiso University, Valparaiso, Indiana 46383, USA  
<sup>47</sup>Variable Energy Cyclotron Centre, Kolkata 700064, India  
<sup>48</sup>Warsaw University of Technology, Warsaw, Poland  
<sup>49</sup>University of Washington, Seattle, Washington 98195, USA  
<sup>50</sup>Wayne State University, Detroit, Michigan 48201, USA  
<sup>51</sup>Institute of Particle Physics, CCNU (HZNU), Wuhan 430079, China  
<sup>52</sup>Yale University, New Haven, Connecticut 06520, USA  
<sup>53</sup>University of Zagreb, Zagreb, HR-10002, Croatia

(Dated: October 24, 2018)

We present a systematic analysis of two-pion interferometry in Au+Au collisions at  $\sqrt{s_{NN}} = 62.4$  GeV and Cu+Cu collisions at  $\sqrt{s_{NN}} = 62.4$  and 200 GeV using the STAR detector at RHIC. The multiplicity and transverse momentum dependences of the extracted correlation lengths (radii) are studied. The scaling with charged particle multiplicity of the apparent system volume at final interaction is studied for the RHIC energy domain. The multiplicity scaling of the measured correlation radii is found to be independent of colliding system and collision energy.

**I. INTRODUCTION**

or density [1] strongly interacting matter will be in a

One of the definitive predictions of quantum chromodynamics (QCD) is that at sufficiently high temperature

state with colored degrees of freedom, i.e. quarks and gluons. The central goal of the experiments with relativistic heavy ion collisions is to create and study this hypothesized form of matter, called the quark-gluon plasma (QGP), which might have existed in the microsecond old universe. Numerous experimental observables have been proposed as signatures of QGP creation in heavy ion collisions [2]. One of these predictions is based on the expectation that the increased number of degrees of freedom associated with the color deconfined state increases the entropy of the system which should survive subsequent hadronization and freeze-out (final interactions). The increased entropy is expected to lead to an increased spatial extent and duration of particle emission, thus providing a significant probe for the QGP phase transition [3, 4].

The information about the space-time structure of the emitting source can be extracted with intensity interferometry techniques [5]. This method, popularly known as Hanbury Brown and Twiss (HBT) correlations, was originally developed to measure angular sizes of stars [6]. The momentum correlations of the produced particles from hadronic sources however include dynamical as well as interference effects, hence the term *femtoscopy* [7] is more appropriate. The primary goal of femtoscopy, performed at mid-rapidity and low transverse momentum, is to study the space-time size of the emitting source and freeze-out processes of the dynamically evolving collision system. Femtoscopic correlations have been successfully studied in most of the heavy ion experiments (see [8] for a recent review).

Experimentally, the two-particle correlation function is the ratio,

$$C(\vec{q}, \vec{K}) = \frac{A(\vec{q}, \vec{K})}{B(\vec{q}, \vec{K})}, \quad (1)$$

where  $A(\vec{q}, \vec{K})$  is the distribution of pairs of particles with relative momentum  $\vec{q} = \vec{p}_1 - \vec{p}_2$  and average momentum  $\vec{K} = (\vec{p}_1 + \vec{p}_2)/2$  from the same event, and  $B(\vec{q}, \vec{K})$  is the corresponding distribution for pairs of particles taken from different events [9, 10]. The correlation function is normalized to unity at large  $\vec{q}$ . With the availability of high statistics data and development of new techniques, it has become possible to measure three-dimensional decompositions of  $\vec{q}$  [11, 12, 13], providing better insight into the collision geometry.

Previous femtoscopic measurements at RHIC in Au+Au collisions at  $\sqrt{s_{NN}} = 130$  GeV [14, 15] and 200 GeV [16, 17] obtained qualitatively similar source sizes. However, detailed comparisons with smaller colliding systems and energies are required in order to understand the dynamics of the source during freeze-out. The crucial information provided from such femtoscopic studies with pions will help to improve our understanding of the reaction mechanisms and to constrain theoretical models of heavy ion collisions [18, 19, 20, 21, 22, 23, 24, 25].

In this paper we present a systematic analysis of two-pion interferometry in Au+Au collisions at  $\sqrt{s_{NN}} =$

62.4 GeV and Cu+Cu collisions at  $\sqrt{s_{NN}} = 62.4$  GeV and 200 GeV using the Solenoidal Tracker at RHIC (STAR) detector at the Relativistic Heavy Ion Collider (RHIC). The article is organized as follows : Section II explains the detector set-up, along with the necessary event, particle and pair cuts. In Section III, the analysis and construction of the correlation function is discussed. The presented results are compared with previous STAR measurements for Au+Au collisions at  $\sqrt{s_{NN}} = 200$  GeV in Section IV. This section also includes a compilation of freeze-out volume estimates for all available heavy ion results from AGS, SPS and RHIC. Section V contains a summary and conclusions.

## II. EXPERIMENTAL SETUP, EVENT AND PARTICLE SELECTION

### A. The STAR detector and Trigger details

The STAR detector [26], which has a large acceptance and is azimuthally symmetric, consists of several detector sub-systems and a solenoidal magnet. In the present study the central Time Projection Chamber (TPC) [27] provided the main information used for track reconstruction. It is 4.2 m long and 4 m in diameter. The TPC covers the pseudo-rapidity region  $|\eta| < 1.8$  with full azimuthal coverage ( $-\pi < \phi < \pi$ ). It is a gas chamber filled with P10 gas (10% methane, 90% argon) with inner and outer radii of 50 and 200 cm, respectively, in a uniform electric field of  $\sim 135$  V/cm. The paths of the particles passing through the gas are reconstructed from the release of secondary electrons that drift to the readout end caps at both ends of the chamber. The readout system is based on multi-wire proportional chambers with cathode pads. There are 45 pad-rows between the inner and outer radii of the TPC.

A minimum bias trigger is obtained using the charged particle hits from an array of scintillator slats arranged in a barrel, called the Central Trigger Barrel, surrounding the TPC, two Zero-Degree Calorimeters (ZDCs) [28] at  $\pm 18$  m from the detector center along the beam line, and two Beam-Beam Counters. The ZDCs measure neutrons at beam rapidity which originate from the break-up of the colliding nuclei. The centrality determination which is used in this analysis is the uncorrected multiplicity of charged particles in the pseudo-rapidity region  $|\eta| < 0.5$  ( $N_{ch}^{TPC}$ ) as measured by the TPC.

### B. Event and Centrality Selection

For this analysis we selected events with a collision vertex within  $\pm 30$  cm measured along the beam axis from the center of the TPC. This event selection is applied to all the data sets discussed here.

The events are further binned according to collision centrality which is determined by the measured charged

TABLE I: Collision centrality selection in terms of percentage of total Au-Au inelastic cross-section, number tracks in TPC, average number of participating nucleons and average number of binary nucleon-nucleon collisions for Au+Au at  $\sqrt{s_{NN}} = 62.4$  GeV.

% cross-section	$N_{ch}^{TPC}$	$\langle N_{part} \rangle$	$\langle N_{coll} \rangle$
0-5	>373	$347.3^{+4.3}_{-3.7}$	$904^{+67.7}_{-62.4}$
5-10	372-313	$293.3^{+7.3}_{-5.6}$	$713.7^{+63.7}_{-54.8}$
10-20	312-222	$229.0^{+9.2}_{-7.7}$	$511.8^{+54.9}_{-48.2}$
20-30	221-154	$162.0^{+10.0}_{-9.5}$	$320.9^{+43.0}_{-39.2}$
30-40	153-102	$112.0^{+9.6}_{-9.1}$	$193.5^{+30.4}_{-31.4}$
40-50	101-65	$74.2^{+9.0}_{-8.5}$	$109.3^{+22.1}_{-21.8}$
50-60	64-38	$45.8^{+7.0}_{-7.1}$	$56.6^{+15.0}_{-14.3}$
60-70	37-20	$25.9^{+5.6}_{-5.6}$	$26.8^{+8.8}_{-9.0}$
70-80	19-9	$13.0^{+3.4}_{-4.6}$	$11.2^{+3.7}_{-4.8}$

TABLE II: Collision centrality selection in terms of percentage of total Cu-Cu inelastic cross-section, number tracks in TPC, average number of participating nucleons and average number of binary nucleon-nucleon collisions for Cu+Cu at  $\sqrt{s_{NN}} = 200$  GeV.

% cross-section	$N_{ch}^{TPC}$	$\langle N_{part} \rangle$	$\langle N_{coll} \rangle$
0-10	>139	$99.0^{+1.5}_{-1.2}$	$188.8^{+15.4}_{-13.4}$
10-20	138-98	$74.6^{+1.3}_{-1.0}$	$123.6^{+9.4}_{-8.3}$
20-30	97-67	$53.7^{+0.9}_{-0.7}$	$77.6^{+5.4}_{-4.7}$
30-40	66-46	$37.8^{+0.7}_{-0.5}$	$47.7^{+2.8}_{-2.7}$
40-50	45-30	$26.2^{+0.5}_{-0.4}$	$29.2^{+1.6}_{-1.4}$
50-60	29-19	$17.2^{+0.4}_{-0.2}$	$16.8^{+0.7}_{-0.7}$

hadron multiplicity within the pseudo-rapidity range  $|y| < 0.5$ . In Table I we list the centrality bins for Au+Au at  $\sqrt{s_{NN}} = 62.4$  GeV along with the multiplicity bin definitions, average number of participating nucleons and average number of binary nucleon-nucleon collisions [29, 30]. For the present analysis we chose six centrality bins corresponding to 0-5%, 5-10%, 10-20%, 20-30%, 30-50%, 50-80% of the total inelastic nucleus-nucleus hadronic cross-section. A dataset of 2 million minimum-bias trigger events which passed the event cuts is used in the analysis.

Tables II and III list the six centrality bins for Cu+Cu

TABLE III: Collision centrality selection in terms of percentage of total Cu-Cu inelastic cross-section, number tracks in TPC, average number of participating nucleons and average number of binary nucleon-nucleon collisions for Cu+Cu at  $\sqrt{s_{NN}} = 62.4$  GeV.

% cross-section	$N_{ch}^{TPC}$	$\langle N_{part} \rangle$	$\langle N_{coll} \rangle$
0-10	>101	$96.4^{+1.1}_{-2.6}$	$161.8^{+12.1}_{-13.5}$
10-20	100-71	$72.1^{+0.6}_{-1.9}$	$107.5^{+6.3}_{-8.6}$
20-30	70-49	$51.8^{+0.5}_{-1.2}$	$68.4^{+3.6}_{-4.7}$
30-40	48-33	$36.2^{+0.4}_{-0.8}$	$42.3^{+1.9}_{-2.6}$
40-50	32-22	$24.9^{+0.4}_{-0.6}$	$25.9^{+1.0}_{-1.5}$
50-60	21-14	$16.3^{+0.4}_{-0.3}$	$15.1^{+0.6}_{-0.6}$

at  $\sqrt{s_{NN}} = 200$  GeV and 62.4 GeV corresponding to 0-10%, 10-20%, 20-30%, 30-40%, 40-50%, 50-60% of the total hadronic cross-section. The number of events used is 15 million and 24 million for 62.4 GeV and 200 GeV Cu+Cu datasets, respectively, after the event cuts.

### C. Particle Selection

We selected particle tracks in the rapidity region  $|y| < 0.5$ . Particle identification was performed by correlating the specific ionization of particles in the TPC gas with their measured momenta. For this analysis pions are selected by requiring the specific ionization to be within 2 standard deviations from their theoretical Bichsel value [31, 32]. In order to remove the kaons and protons which could satisfy this condition, particles are also required to be more than 2 standard deviations from the Bethe-Bloch value for kaons and protons. Charged particle tracks reconstructed and used for this analysis are accepted if they have space points on at least 15 pad rows in TPC. Tracks with fewer space points may be broken track fragments. These cuts are similar to those in our previous analysis of Au+Au collisions at  $\sqrt{s_{NN}} = 200$  GeV [17] since the detector setup was identical.

### D. Pair Cuts

Two types of particle track reconstruction errors directly affect measured particle pair densities at the small relative momentum values studied here. Track splitting, in which one particle trajectory is reconstructed as two or more “particles,” increases the apparent number of pairs at low relative  $q$ . To address this problem we developed a split track filter algorithm, described in our previous analysis of Au+Au collisions at  $\sqrt{s_{NN}} = 200$  GeV [17],

where values of the splitting level parameter from  $-0.5$  to  $0.6$  [17] ensured valid tracks. The inefficiencies arising due to track merging, in which two or more particle trajectories are reconstructed as one track, was completely eliminated by requiring that the fraction of merged hits (overlapping space-charge depositions in the TPC gas) be less than 10% for every track pair used in the correlation function.

In the present analysis, we used the same cuts to remove splitting and merging as were used for Au+Au collisions at  $\sqrt{s_{\text{NN}}} = 200$  GeV [17]. The track pairs are required to have an average transverse momentum ( $k_{\text{T}} = (|\vec{p}_{1\text{T}} + \vec{p}_{2\text{T}}|)/2$ ) in one of 4 bins corresponding to [150,250] MeV/c, [250,350] MeV/c, [350,450] MeV/c and [450,600] MeV/c. The results are presented and discussed as a function of  $k_{\text{T}}$  and  $m_{\text{T}}$  ( $= \sqrt{k_{\text{T}}^2 + m_{\pi}^2}$ ) in each of those bins.

### III. ANALYSIS METHOD

#### A. Correlation function

The numerator and denominator of the two particle correlation function in Eq.(1) are constructed by filling histograms corresponding to particle pairs from the same event and from mixed events, respectively. The background pairs are constructed from mixed events [9] where by pairing each particle in a given event is mixed with all particles from other events within a subset of ten similar events. The events for mixing are selected within the given centrality bin such that their respective primary vertex  $z$  positions are all within 10 cm of one another.

#### B. Bertsch-Pratt Parametrizations and Coulomb interactions

We decompose the relative momentum  $\vec{q}$  according to the Bertsch-Pratt (or “out-side-long”) convention [11, 12, 13, 33, 34]. The relative momentum  $\vec{q}$  is decomposed into the variables  $q_{\text{long}}$  along the beam direction,  $q_{\text{out}}$  parallel to the transverse momentum of the pair  $\vec{k}_{\text{T}} = (\vec{p}_{1\text{T}} + \vec{p}_{2\text{T}})/2$ , and  $q_{\text{side}}$  perpendicular to  $q_{\text{long}}$  and  $q_{\text{out}}$ .

In addition to the correlation arising from the quantum statistics of two identical (boson) particles, correlations can also arise from two-particle final state interactions even for non-identical particles [35, 36, 37]. For identical pions the effects of strong interactions are negligible, but the long range Coulomb repulsion causes a suppression of the measured correlation function at small  $\vec{q}$ .

In this paper we follow the procedure used in our previous analysis of Au+Au collisions at  $\sqrt{s_{\text{NN}}} = 200$  GeV [17]. For an azimuthally integrated analysis at mid-rapidity in the longitudinal co-moving system (LCMS) the correlation function in Eq. (1) can be decomposed

as [8, 38]:

$$C(q_{\text{out}}, q_{\text{side}}, q_{\text{long}}) = (1-\lambda) +$$

$$\lambda K_{\text{Coul}}(q_{\text{inv}})(1 + e^{-q_{\text{out}}^2 R_{\text{out}}^2 - q_{\text{side}}^2 R_{\text{side}}^2 - q_{\text{long}}^2 R_{\text{long}}^2}), \quad (2)$$

where  $K_{\text{Coul}}$  is, to a good approximation, the squared nonsymmetrized Coulomb wave function integrated over a Gaussian source (corresponding to the LCMS Gaussian radii  $R_{\text{out}}$ ,  $R_{\text{side}}$ ,  $R_{\text{long}}$ ). Assuming perfect experimental particle identification and a purely chaotic (incoherent) source,  $\lambda$  represents the fraction of correlated pairs [39].

We assumed a spherical Gaussian source of 5 fm for Au+Au collisions at  $\sqrt{s_{\text{NN}}} = 62.4$  GeV and a 3 fm source for Cu+Cu collisions at  $\sqrt{s_{\text{NN}}} = 62.4$  and 200 GeV. The first term  $(1 - \lambda)$  in Eq.(2) accounts for those pairs which do not interact or interfere and the second term represents those pairs where both Bose-Einstein effects and Coulomb interactions are present [17].

#### C. Systematic Uncertainties

We studied several sources of systematic errors similar to a previously published STAR pion interferometry analysis for Au+Au collisions at  $\sqrt{s_{\text{NN}}} = 200$  GeV [17]. The following effects are considered: track merging, track splitting, source size assumed for the Coulomb correction, particle identification purity, and particle pair acceptance effects for unlike-sign charged pions. The estimated systematic errors are less than 10% for  $R_{\text{out}}$ ,  $R_{\text{side}}$ ,  $R_{\text{long}}$ ,  $\lambda$  in all centrality and  $k_{\text{T}}$  bins for the present datasets and are similar to those in [17]. This similarity is expected since the detector setup was identical and similar particle and pair selection cuts are used for Au+Au and Cu+Cu collisions. Results shown in the figures for the present datasets include statistical errors only.

### IV. RESULTS AND DISCUSSION

#### A. Au+Au collisions at $\sqrt{s_{\text{NN}}} = 62.4$ GeV

The correlation function in Eq.(2) is fitted to the 3D correlation data for Au+Au collisions at  $\sqrt{s_{\text{NN}}} = 62.4$  GeV for each centrality and  $m_{\text{T}}$  bins as defined above. The analysis is performed separately for  $\pi^+\pi^+$  and  $\pi^-\pi^-$  pairs. The final histograms for the like-sign pairs do not show appreciable differences and may therefore be summed in order to increase statistics. Figure 1 presents the results for  $R_{\text{out}}$ ,  $R_{\text{side}}$ ,  $R_{\text{long}}$ ,  $\lambda$  and the ratio,  $R_{\text{out}}/R_{\text{side}}$ . The three femtoscopic radii increase with increasing centrality as expected, whereas the values of  $\lambda$  and the  $R_{\text{out}}/R_{\text{side}}$  ratio exhibit no clear centrality dependences.

We observe that for all centralities the three femtoscopic radii decrease with increasing  $m_{\text{T}}$  whereas the  $\lambda$

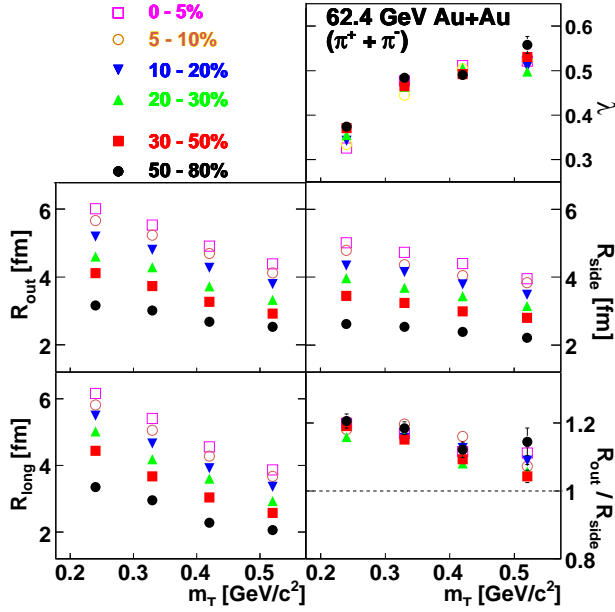


FIG. 1: (Color Online) The femtoscopic parameters vs.  $m_T$  for 6 different centralities for Au+Au collisions at  $\sqrt{s_{NN}} = 62.4$  GeV. Only statistical errors are shown. The estimated systematic errors are less than 10% for  $R_{out}$ ,  $R_{side}$ ,  $R_{long}$ ,  $\lambda$  in all centrality and  $k_T$  bins.

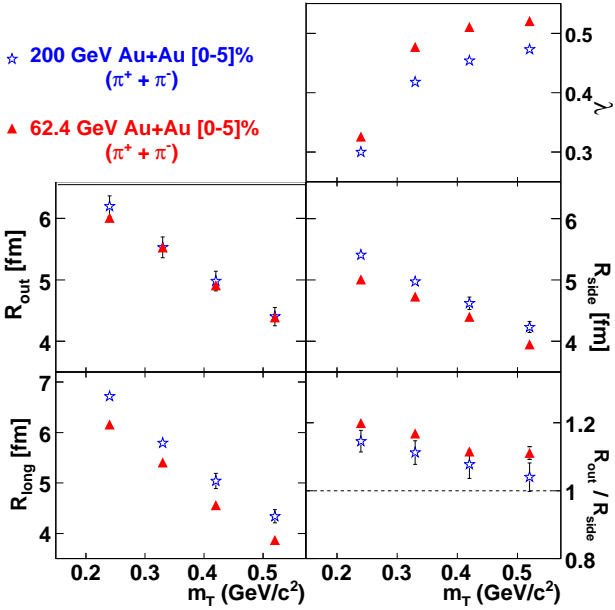


FIG. 2: (Color Online) The comparison of femtoscopic measurements of Au+Au collisions at  $\sqrt{s_{NN}} = 200$  GeV and 62.4 GeV for 0-5% most central events. Only statistical errors are shown for Au+Au collisions at  $\sqrt{s_{NN}} = 62.4$  GeV. The estimated systematic errors for Au+Au collisions at  $\sqrt{s_{NN}} = 62.4$  GeV are less than 10% for  $R_{out}$ ,  $R_{side}$ ,  $R_{long}$ ,  $\lambda$  in 0-5% most central events and all  $k_T$  bins. The 200 GeV results are from [17].

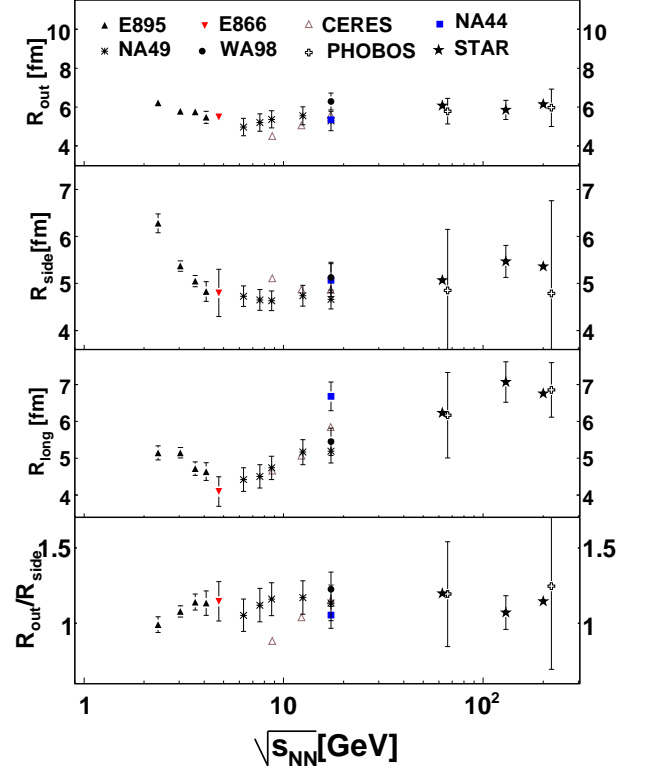


FIG. 3: (Color Online) The energy dependence of femtoscopic parameters for AGS, SPS and RHIC from Refs. [14, 17, 50, 51, 52, 53, 54, 55, 56, 57]. Energy dependences of pion femtoscopic parameters for central Au+Au, Pb+Pb and Pb+Au collisions are shown for mid-rapidity and  $\langle k_T \rangle \sim 0.2-0.3$  GeV/c. Error bars on NA44, NA49, CERES, PHOBOS and STAR results at  $\sqrt{s_{NN}} = 130$  and 200 GeV include systematic uncertainties; error bars on other results are statistical only. Only statistical errors are shown for Au+Au collisions at  $\sqrt{s_{NN}} = 62.4$  GeV; the estimated systematic errors are less than 10% for  $R_{out}$ ,  $R_{side}$ ,  $R_{long}$ . The PHOBOS results from [50] for  $\sqrt{s_{NN}} = 62.4$  and 200 GeV are slightly shifted horizontally for visual clarity.

parameter increases with  $m_T$ . Such behavior is consistent with our previous measurements at  $\sqrt{s_{NN}} = 200$  GeV [17]. The increase of parameter  $\lambda$  with  $m_T$  is due to the decreasing contribution of pions produced from long-lived resonance decays at higher transverse momenta. For comparison, in Fig. 2 we show the results for Au+Au collisions at  $\sqrt{s_{NN}} = 62.4$  GeV and 200 GeV for the most central collisions. We observe that the  $R_{out}$  values are similar for both cases, but there are differences between the values of  $R_{side}$  and  $R_{long}$ . The  $R_{out}/R_{side}$  ratio decreases with increasing  $m_T$ , but the values are higher for  $\sqrt{s_{NN}} = 62.4$  GeV than for  $\sqrt{s_{NN}} = 200$  GeV.

The observed dependences of the three femtoscopic radii are qualitatively consistent with models with collective flow [40, 41, 42]. Collective expansion results in position-momentum correlations in both transverse and longitudinal directions. In an expanding source

the correlation between the space-time points where the pions are emitted and their energy-momentum produce a characteristic dependence of femtoscopic radii on  $m_T$  [8, 12, 22, 43, 44, 45, 46, 47, 48]. The decrease in the “out” and “side” components can be described by models including transverse flow [17, 22, 43, 45], and the decrease in the “long” component by those with longitudinal flow [17, 44, 45, 49].

## B. Energy dependence of femtoscopic radii

In Fig. 3 we present the energy dependences of the three femtoscopic radii and the ratio  $R_{\text{out}}/R_{\text{side}}$  for the available data from AGS, SPS and RHIC. The results are compiled for Au+Au, Pb+Pb and Pb+Au collisions at mid-rapidity and for  $\langle k_T \rangle \sim 0.2\text{-}0.3$  GeV/c. The present measurements for Au+Au collisions at  $\sqrt{s_{\text{NN}}} = 62.4$  GeV are also included. The quality of the present STAR data with respect to statistical and systematic errors is significantly better than that reported by PHOBOS [50] at the same energy. PHENIX results are not included because they were reported for broader centrality bins. WA97 results are also omitted because they were measured at higher transverse momenta.

Comparative studies are a necessary part of searches for nontrivial structures in the excitation function which might arise from a possible phase transition [3]. The radius parameter  $R_{\text{side}}$  has the most direct correlation with the source geometry whereas  $R_{\text{out}}$  encodes both geometry and time scale information. Experimental results show that  $R_{\text{side}}$  decreases at AGS energies and then displays a modest rise with collision energy from SPS to RHIC.  $R_{\text{long}}$  increases with collision energy after an initial decrease at the lower AGS energies. For  $R_{\text{out}}$  the changes are very small.

Hydrodynamic model calculations [3, 4] predict an enhancement in the ratio of  $R_{\text{out}}/R_{\text{side}}$  with increasing beam energy. The experimental results show no such behavior. The measured ratios are better reproduced by the AMPT (A Multi-Phase Transport) model [58], however the individual predicted radii have a steeper decrease compared to the experimental data [8]. An alternative model using a relativistic quantum mechanical treatment of opacity and the refractive index is capable of reproducing the observed results [59], but strongly depends on the assumed initial conditions and neglects the time dependence of the corresponding optical potential. Hydrodynamic calculations [60] including viscosity offer another possible explanation for the above deviation between the data and model calculations as recently shown in [61]. According to recent hydrodynamic calculations, the femtoscopic radii can be described either by using the initial Gaussian density profile [62] or by including the combination of several effects including: pre-thermal acceleration, a stiffer equation of state, and additional viscous corrections [63]. Other recent studies with a granular source model [64] also obtain a better description of the

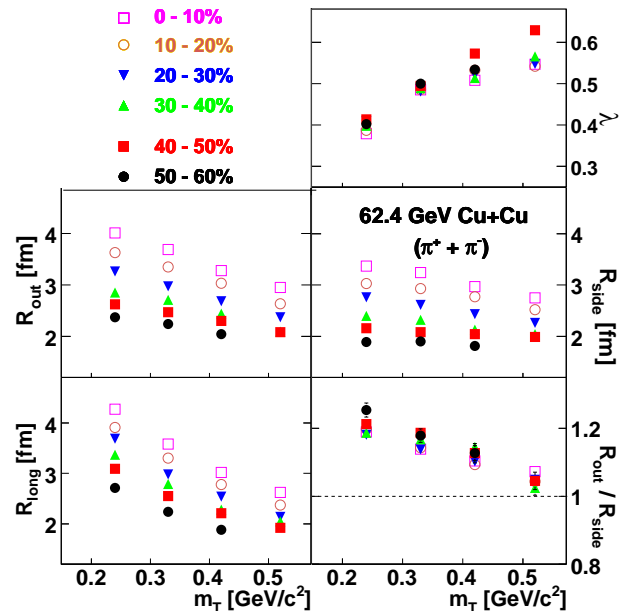


FIG. 4: (Color Online) Femtoscopic parameters vs.  $m_T$  for six centralities for Cu+Cu collisions at  $\sqrt{s_{\text{NN}}} = 62.4$  GeV. Only statistical errors are shown. The estimated systematic errors are less than 10% for  $R_{\text{out}}$ ,  $R_{\text{side}}$ ,  $R_{\text{long}}$ ,  $\lambda$  in all centrality and  $k_T$  bins.

experimental measurements of pion femtoscopic radii.

## C. Cu+Cu collisions at $\sqrt{s_{\text{NN}}} = 62.4$ and 200 GeV

The correlation functions are similarly constructed for Cu+Cu collisions at  $\sqrt{s_{\text{NN}}} = 62.4$  GeV and 200 GeV. The extracted femtoscopic radii,  $R_{\text{out}}$ ,  $R_{\text{side}}$  and  $R_{\text{long}}$ , along with the  $\lambda$  parameter and the ratio  $R_{\text{out}}/R_{\text{side}}$  are presented in Figs. 4 and 5 for the 62.4 and 200 GeV data, respectively. The results are presented for six different centralities and four  $m_T$  bins. The highest  $k_T$  bin [450 - 600] MeV/c of the most peripheral centrality (50 - 60 %) in Cu+Cu collisions at  $\sqrt{s_{\text{NN}}} = 62.4$  GeV is omitted due to inadequate statistics for decomposition with the Bertsch-Pratt parametrization. For both collision energies the three femtoscopic radii increase with increasing centrality whereas the  $\lambda$  parameter shows no centrality dependence. The  $m_T$  dependences of the femtoscopic radii are similar to that for Au+Au collisions. The  $R_{\text{out}}/R_{\text{side}}$  ratios exhibit no clear centrality dependences for either energy.

## D. Comparison of femtoscopic radii for Cu+Cu and Au+Au collisions

In Fig. 6 the femtoscopic source parameters  $\lambda$ ,  $R_{\text{out}}$ ,  $R_{\text{side}}$ ,  $R_{\text{long}}$  and the ratio  $R_{\text{out}}/R_{\text{side}}$  for central (0-5%) Au+Au collisions at  $\sqrt{s_{\text{NN}}} = 200$  GeV [17] are compared

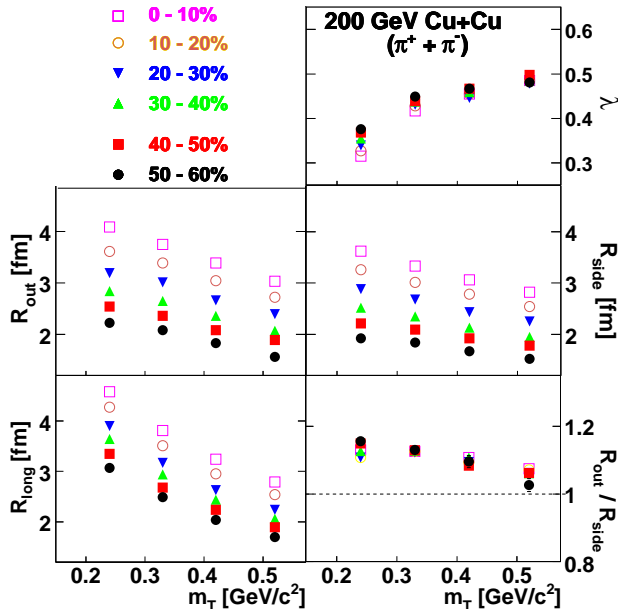


FIG. 5: (Color Online) Femsotopic parameters vs.  $m_T$  for six centralities for Cu+Cu collisions at  $\sqrt{s_{NN}} = 200$  GeV. Only statistical errors are shown. The estimated systematic errors are less than 10% for  $R_{out}$ ,  $R_{side}$ ,  $R_{long}$ ,  $\lambda$  in all centrality and  $k_T$  bins.

with central (0-10%) Cu+Cu collisions at same beam energy. As expected, the femsotopic radii for Cu+Cu collisions are smaller than for Au+Au collisions at the same beam energy. It is interesting that the values of the ratio  $R_{out}/R_{side}$  for the two systems are similar.

In Fig. 7 we extend the comparison of femsotopic source parameters to include central (0-5%) Au+Au collisions at  $\sqrt{s_{NN}} = 62.4$  GeV, central (0-10%) Cu+Cu collisions at  $\sqrt{s_{NN}} = 62.4$  and 200 GeV, and central (0-15%)  $\pi^+\pi^+$  and  $\pi^-\pi^-$  correlations from Au+Au collisions at 62.4 GeV from the PHOBOS experiment [50]. The femsotopic radii for Cu+Cu collisions at  $\sqrt{s_{NN}} = 62.4$  GeV are smaller than those for Au+Au collisions at the same beam energy. The femsotopic radii for Cu+Cu central collisions are similar for both energies. The variation of the  $R_{out}/R_{side}$  ratio with  $m_T$  is similar for the Au+Au and Cu+Cu collision data.

In Fig. 8 we present the  $m_T$  dependences of the ratios of femsotopic radii for the most-central Au+Au and Cu+Cu collisions at  $\sqrt{s_{NN}} = 200$  and 62.4 GeV. Ratios for the same colliding ion systems are close to unity whereas ratios of radii for Au+Au to Cu+Cu collisions are  $\sim 1.5$ . Although the individual radii decrease significantly with increasing  $m_T$  the ratios in Fig. 8 show that the femsotopic radii for Au+Au and Cu+Cu collisions at 62.4 and 200 GeV share a common  $m_T$  dependence. This result can be understood in terms of models [59, 65] which use participant scaling to predict the femsotopic radii in Cu+Cu collisions from the measured radii for Au+Au collisions at  $\sqrt{s_{NN}} = 200$  GeV, assuming the

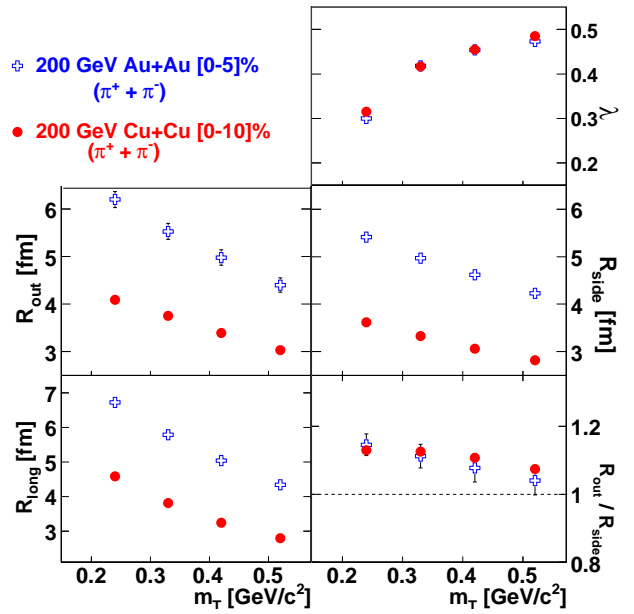


FIG. 6: (Color Online) The comparison of system size dependence in femsotopic measurements of STAR Au+Au and Cu+Cu collisions at  $\sqrt{s_{NN}} = 200$  GeV. Only statistical errors are shown for Cu+Cu collisions at  $\sqrt{s_{NN}} = 200$  GeV. The estimated systematic errors for Cu+Cu collisions at  $\sqrt{s_{NN}} = 200$  GeV are less than 10% for  $R_{out}$ ,  $R_{side}$ ,  $R_{long}$ ,  $\lambda$  in 0-10% most central events and  $k_T$  bins. The Au+Au results are from [17].

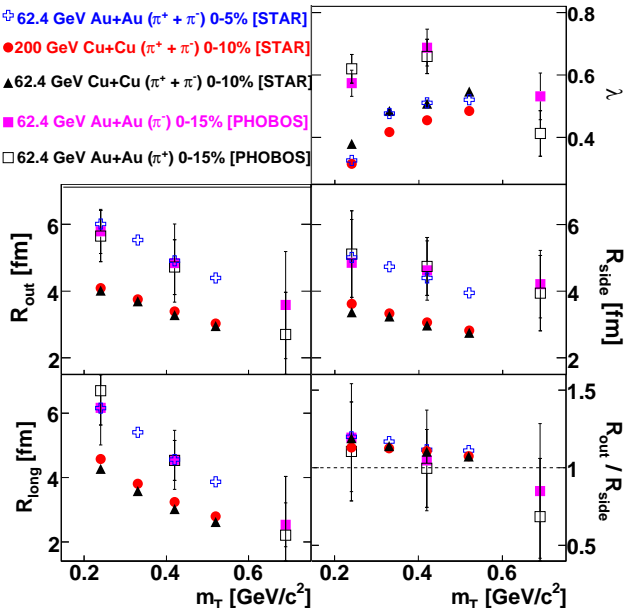


FIG. 7: (Color Online) The comparison of femsotopic measurements of STAR Cu+Cu collisions at  $\sqrt{s_{NN}} = 200$  and 62.4 GeV and Au+Au collisions at  $\sqrt{s_{NN}} = 62.4$  GeV. Only statistical errors are shown for STAR results. The estimated systematic errors for STAR results are less than 10% for  $R_{out}$ ,  $R_{side}$ ,  $R_{long}$ ,  $\lambda$  in all centrality and  $k_T$  bins. The PHOBOS results [50] for positive and negative pions in Au+Au collisions at  $\sqrt{s_{NN}} = 62.4$  GeV are compared with STAR results.

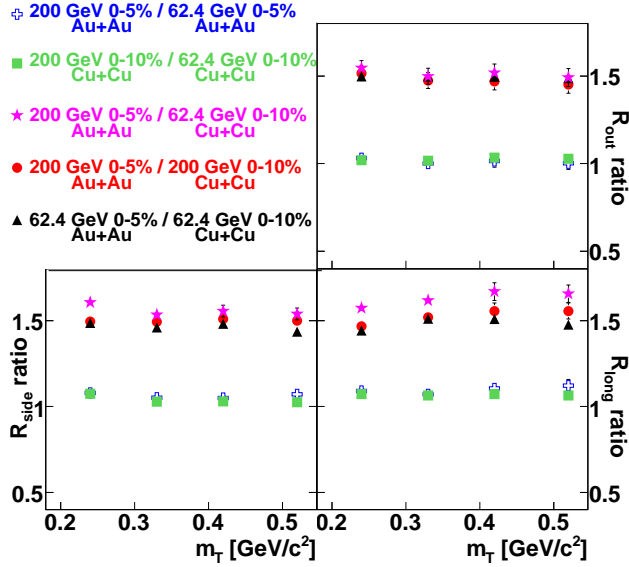


FIG. 8: (Color Online) Ratios of femtosopic radii at top centralities for Au+Au and Cu+Cu collisions at  $\sqrt{s_{NN}} = 200$  and 62.4 GeV vs.  $m_T$ . Only statistical errors are shown for Au+Au collisions at  $\sqrt{s_{NN}} = 62.4$  GeV and Cu+Cu collisions at  $\sqrt{s_{NN}} = 62.4$  and 200 GeV. The estimated systematic errors for Au+Au collisions at  $\sqrt{s_{NN}} = 62.4$  GeV and Cu+Cu collisions at  $\sqrt{s_{NN}} = 62.4$  and 200 GeV are less than 10% for  $R_{out}$ ,  $R_{side}$ ,  $R_{long}$  in all centrality and  $k_T$  bins. The 200 GeV results are from [17].

radii are proportional to  $A^{1/3}$ , where A is the atomic mass number of the colliding nuclei.

### E. Volume estimates and multiplicity scaling

Estimates of the pion freeze-out volume  $V_f$  in terms of the femtosopic radii are provided by the following expressions:

$$V_f \propto R_{side}^2 R_{long} \quad (3a)$$

$$V_f \propto R_{out} R_{side} R_{long}. \quad (3b)$$

However, the correlation lengths (femtoscopic radii) decrease with increasing  $m_T$  corresponding to an  $m_T$  dependent region of homogeneity which, in expanding source models, is smaller than the true collision volume at freeze-out. The volume estimates [Eqs. (3a) and (3b)] are obtained from the lowest  $m_T$  bin, corresponding to the  $k_T$  region from 150 to 250 MeV/c as discussed in Sec. (IID).

The  $V_f$  measurements using Eq. (3a) as a function of  $\sqrt{s_{NN}}$  are presented in Fig. 9 for Au+Au, Pb+Pb and Pb+Au collisions at mid-rapidity and for the lowest  $k_T$  bin defined above. The results show two distinct domains: First, at the AGS where the volume measure de-

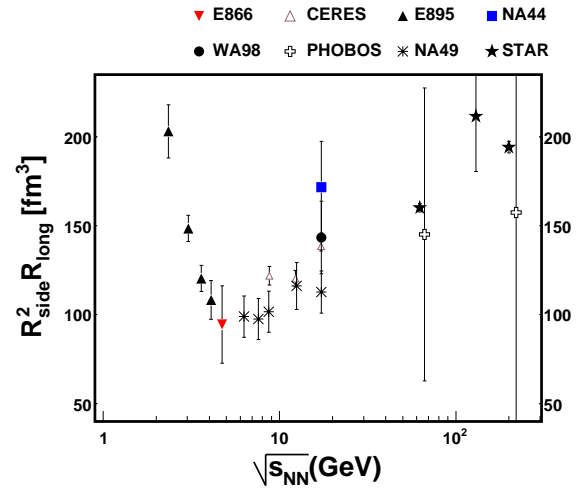


FIG. 9: (Color Online) The energy dependence of the pion freeze-out volume for heavy ion collision data from the AGS, SPS and RHIC estimated using Eq. (3a). The references are given in the caption of Fig. 3. Only statistical errors are shown for Au+Au collisions at  $\sqrt{s_{NN}} = 62.4$  GeV. The estimated systematic errors for Au+Au collisions at  $\sqrt{s_{NN}} = 62.4$  GeV are less than 10% for  $R_{out}$ ,  $R_{side}$ ,  $R_{long}$  in all centrality and  $k_T$  bins.

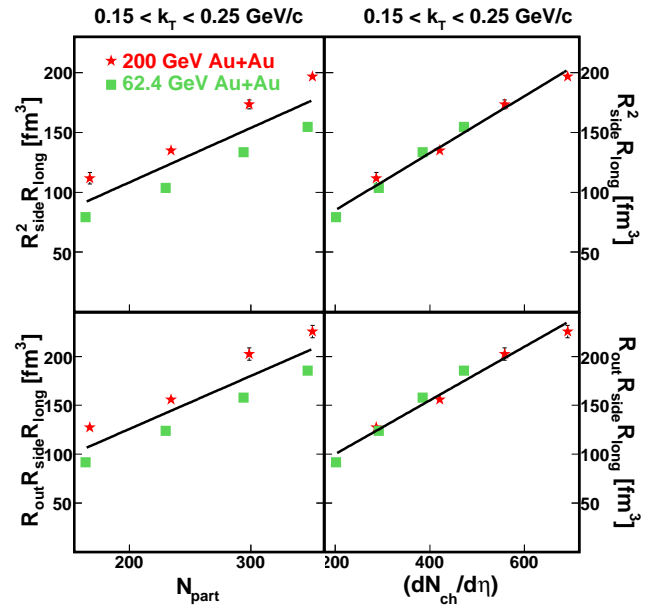


FIG. 10: (Color Online) Pion freeze-out volume estimates as a function of number of participants and charged particle multiplicity density for Au+Au at  $\sqrt{s_{NN}} = 200$  and 62.4 GeV. Only statistical errors are shown for Au+Au collisions at  $\sqrt{s_{NN}} = 62.4$  GeV. The estimated systematic errors for Au+Au collisions at  $\sqrt{s_{NN}} = 62.4$  GeV are less than 10% for  $R_{out}$ ,  $R_{side}$ ,  $R_{long}$  in all centrality and  $k_T$  bins. The 200 GeV Au+Au collision results are from [17]. The lines in each panel represent linear fits to the data.

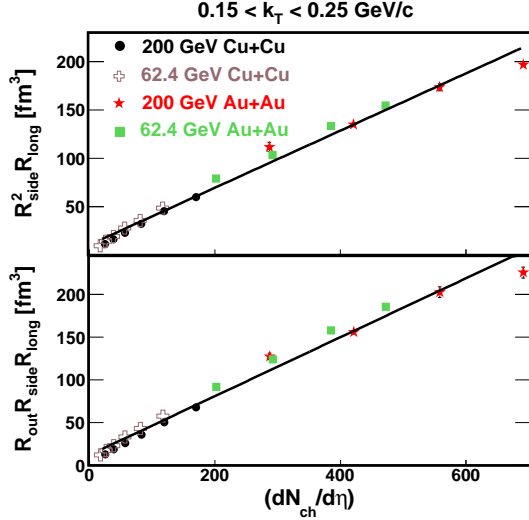


FIG. 11: (Color Online) Pion freeze-out volume estimates as a function of charged particle multiplicity density for Au+Au and Cu+Cu collisions. Only statistical errors are shown for Au+Au collisions at  $\sqrt{s_{NN}} = 62.4$  GeV and Cu+Cu collisions at  $\sqrt{s_{NN}} = 62.4$  and 200 GeV. The estimated systematic errors for Au+Au collisions at  $\sqrt{s_{NN}} = 62.4$  GeV and Cu+Cu collisions at  $\sqrt{s_{NN}} = 62.4$  and 200 GeV are less than 10% for  $R_{out}$ ,  $R_{side}$ ,  $R_{long}$  in all centrality and  $k_T$  bins. The 200 GeV Au+Au collision results are from [17]. The lines in each panel represent linear fits to the data.

creases, and second, in the SPS and RHIC energy regimes where a monotonic increase is observed.

A detailed description of this non-trivial behavior was suggested in [66] based on the hypothesis of constant mean free path length of pions at freeze-out. The explanation provided in [66] defines the pion mean free path length,  $\lambda_f$ , as:

$$\lambda_f = \frac{1}{\rho_f \sigma} = \frac{V_f}{N\sigma}, \quad (4)$$

where  $\rho_f$  is the freeze-out density and  $\sigma$  is the total cross-section for pions to interact with the surrounding medium. The freeze-out density can be expressed as the number of particles  $N$  in the estimated freeze-out volume  $V_f$ , divided by  $V_f$ , resulting in the second expression in Eq. (4). The denominator,  $N\sigma$ , can be expanded as the sum of the pion-pion and pion-nucleon contributions. At AGS energies the pion-nucleon term dominates since the pion-nucleon cross-section is larger than the pion-pion cross-section. Also, the number of nucleons at these lower energies at mid-rapidity exceeds the number of pions. Hence, a decrease in the number of mid-rapidity nucleons leads to a decrease in the observed freeze-out volume ( $V_f$ ) as a function of  $\sqrt{s_{NN}}$ . At SPS and RHIC energies the pion-pion term dominates the denominator in Eq. (4) due to copious pion production leading to an increase in the observed  $V_f$ .

Based on this interpretation we expect the volume estimates in the pion dominated RHIC regime to show a

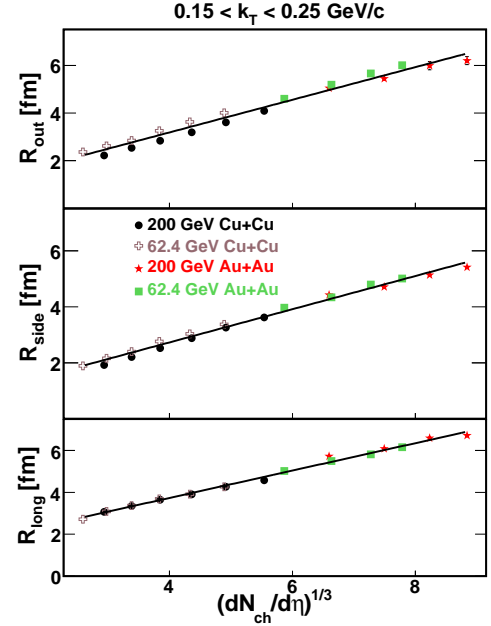


FIG. 12: (Color Online) The pion source radii dependences on charged particle multiplicity density for Au+Au and Cu+Cu collisions. Only statistical errors are shown for Au+Au collisions at  $\sqrt{s_{NN}} = 62.4$  GeV and Cu+Cu collisions at  $\sqrt{s_{NN}} = 62.4$  and 200 GeV. The estimated systematic errors for Au+Au collisions at  $\sqrt{s_{NN}} = 62.4$  GeV and Cu+Cu collisions at  $\sqrt{s_{NN}} = 62.4$  and 200 GeV are less than 10% for  $R_{out}$ ,  $R_{side}$ ,  $R_{long}$  in all centrality and  $k_T$  bins. The 200 GeV Au+Au collision results are from [17]. The lines represent linear fits to the data.

linear dependence on charged particle multiplicity. In Fig. 10 freeze-out volume estimates (using Eqs. (3a) and (3b)) are shown as a function of the number of participants (left panels) and charged particle multiplicity (right panels) for Au+Au collisions at  $\sqrt{s_{NN}} = 62.4$  and 200 GeV. The predicted linear increase with charged particle multiplicity is observed. Estimated freeze-out volumes for Au+Au collisions at the same centralities increase with collision energy indicating that  $N_{part}$  is not a suitable scaling variable in this case. On the other hand, charged particle multiplicity provides better scaling properties.

Additional estimates of freeze-out volume dependences on charged particle multiplicity are presented in Fig. 11 for both the Au+Au and Cu+Cu results at  $\sqrt{s_{NN}} = 62.4$  and 200 GeV. Both freeze-out volume estimates for the four collision systems show an approximate, common linear dependence on charged particle multiplicity. The linear dependences of femtoscopic radii on  $(dN_{ch}/d\eta)^{1/3}$  for Au+Au and Cu+Cu collisions at  $\sqrt{s_{NN}} = 62.4$  and 200 GeV are shown in Fig. 12. The above common, linear dependences [8] are consistent with the assumption of a universal pion mean-free-path length at freeze-out [66].

## V. SUMMARY AND CONCLUSIONS

We have presented systematic measurements of pion femtoscopy for Au+Au collisions at  $\sqrt{s_{NN}} = 62.4$  GeV and Cu+Cu collisions at  $\sqrt{s_{NN}} = 62.4$  and 200 GeV, and compared these new results with our previous analysis of Au+Au collisions at  $\sqrt{s_{NN}} = 200$  GeV [17]. For all the systems considered the three femtosopic radii ( $R_{out}$ ,  $R_{side}$  and  $R_{long}$ ) increase with centrality, whereas the values of the  $\lambda$  parameter and ratio  $R_{out}/R_{side}$  are approximately constant with centrality. The three femtosopic radii decrease with increasing  $m_T$ , whereas the  $\lambda$  parameter increases with  $m_T$ . The increase of  $\lambda$  with  $m_T$  is attributed to decreasing contamination from pions produced from long-lived resonance decays at higher transverse momentum.

The decrease of femtosopic radii with increasing  $m_T$  can be described by models with collective, transverse and longitudinal expansion or flow. The ratios of femtosopic radii at top centralities for different colliding systems (Au+Au and Cu+Cu) at  $\sqrt{s_{NN}} = 62.4$  and 200 GeV show that the corresponding radii vary similarly with  $m_T$ .

The predicted rise of the ratio  $R_{out}/R_{side}$  with collision energy due to a possible phase transition [3] is not observed for Au+Au and Cu+Cu collisions. The compilation of freeze-out volume estimates  $V_f$  as a function of collision energy  $\sqrt{s_{NN}}$  (using Eq. (3a) along with the datasets presented in Fig. 3) shows two distinct domains: with increasing  $\sqrt{s_{NN}}$ ,  $V_f$  decreases at the AGS, but steadily increases throughout the SPS and RHIC energy regimes. At AGS energies the decreasing number of baryons at mid-rapidity leads to a decrease in the observed freeze-out volume ( $V_f$ ) as a function of  $\sqrt{s_{NN}}$ . At higher beam energies from SPS to RHIC copious and increasing pion production causes the freeze-out volume to

rise.

The dependences of the freeze-out volume estimate on number of participants and charged particle multiplicity are compared. Measurements for Au+Au collisions at the same centralities, but different energies yield different freeze-out volumes demonstrating that  $N_{part}$  is not a suitable scaling variable. The freeze-out volume estimates for all four collision systems presented here show a linear dependence on final charged particle multiplicity which is consistent with the hypothesis of a universal mean-free-path length at freeze-out.

For the systems studied here the multiplicity and  $k_T$  dependences of the femtosopic radii are consistent with previously established trends at RHIC and at lower energies. The radii scale with the final state collision multiplicity which, in a static model, is consistent with an hypothesized universal mean-free-path length at freeze-out. This and similar studies establish the baseline systematics against which to compare future femtosopic studies at the LHC [67].

We thank the RHIC Operations Group and RCF at BNL, and the NERSC Center at LBNL and the resources provided by the Open Science Grid consortium for their support. This work was supported in part by the Offices of NP and HEP within the U.S. DOE Office of Science, the U.S. NSF, the Sloan Foundation, the DFG cluster of excellence ‘Origin and Structure of the Universe,’ CNRS/IN2P3, RA, RPL, and EMN of France, STFC and EPSRC of the United Kingdom, FAPESP of Brazil, the Russian Ministry of Sci. and Tech., the NNSFC, CAS, MoST, and MoE of China, IRP and GA of the Czech Republic, FOM of the Netherlands, DAE, DST, and CSIR of the Government of India and the Korea Sci. & Eng. Foundation. We wish to thank Polish State Committee for Scientific Research, grant: N202 013 31/0489.

- 
- [1] J. C. Collins and M. J. Perry, Phys. Rev. Lett. **34**, 1353 (1975); E. V. Shuryak, Phys. Rept. **61** (1980) 71; D. J. Gross, R. D. Pisarski and L. G. Yaffe, Rev. Mod. Phys. **53**, 43 (1981); L. D. McLerran and B. Svetitsky, Phys. Lett. B **98**, 195 (1981).
  - [2] J. Adams *et al.* [STAR Collaboration], Nucl. Phys. A **757**, 102 (2005).
  - [3] D. H. Rischke and M. Gyulassy, Nucl. Phys. A **608**, 479 (1996).
  - [4] D. H. Rischke, Nucl. Phys. A **610**, 88c (1996).
  - [5] G. Goldhaber, S. Goldhaber, W. Y. Lee and A. Pais, Phys. Rev. **120**, 300 (1960).
  - [6] R. Hanbury Brown and R. Q. Twiss, Phil. Mag. **45**, 663 (1954). R. Hanbury Brown and R. Q. Twiss, Nature **178**, 1046 (1956).
  - [7] R. Lednicky, arXiv:nucl-th/0212089.
  - [8] M. A. Lisa, S. Pratt, R. Soltz and U. Wiedemann, Ann. Rev. Nucl. Part. Sci. **55**, 357 (2005).
  - [9] G. I. Kopylov and M. I. Podgoretsky, Sov. J. Nucl. Phys. **15**, 219 (1972) [Yad. Fiz. **15**, 392 (1972)].
  - [10] U. W. Heinz and B. V. Jacak, Ann. Rev. Nucl. Part. Sci. **49**, 529 (1999).
  - [11] G. Bertsch, M. Gong and M. Tohyama, Phys. Rev. C **37**, 1896 (1988).
  - [12] S. Pratt, Phys. Rev. D **33**, 1314 (1986).
  - [13] S. Chapman, P. Scotto and U. W. Heinz, Phys. Rev. Lett. **74**, 4400 (1995).
  - [14] C. Adler *et al.* [STAR Collaboration], Phys. Rev. Lett. **87**, 082301 (2001).
  - [15] K. Adcox *et al.* [PHENIX Collaboration], Phys. Rev. Lett. **88**, 192302 (2002).
  - [16] S. S. Adler *et al.* [PHENIX Collaboration], Phys. Rev. Lett. **93**, 152302 (2004).
  - [17] J. Adams *et al.* [STAR Collaboration], Phys. Rev. C **71**, 044906 (2005).
  - [18] G. Baym, Acta Phys. Polon. B **29**, 1839 (1998).
  - [19] S. S. Padula, Braz. J. Phys. **35**, 70 (2005).
  - [20] E. V. Shuryak, Phys. Lett. B **44**, 387 (1973).
  - [21] L. D. McLerran, FERMILAB-CONF-88-068-T *Presented at Int. Conf. on Physics and Astrophysics of the Quark*

*Gluon Plasma, Bombay, India, Feb 8-12, 1988*

- [22] U. W. Heinz, arXiv:nucl-th/9609029.
- [23] U. A. Wiedemann and U. W. Heinz, Phys. Rept. **319**, 145 (1999).
- [24] U. W. Heinz, Nucl. Phys. A **610**, 264c (1996).
- [25] B. Tomasik and U. A. Wiedemann, arXiv:hep-ph/0210250.
- [26] K. H. Ackermann *et al.* [STAR Collaboration], Nucl. Instrum. Meth. A **499**, 624 (2003).
- [27] K. H. Ackermann *et al.* [STAR Collaboration], Nucl. Phys. A **661**, 681 (1999).
- [28] C. Adler, A. Denisov, E. Garcia, M. J. Murray, H. Strobele and S. White, Nucl. Instrum. Meth. A **470**, 488 (2001).
- [29] J. Adams *et al.* [STAR Collaboration], Phys. Rev. C **73**, 034906 (2006).
- [30] M. L. Miller, K. Reygers, S. J. Sanders and P. Steinberg, Ann. Rev. Nucl. Part. Sci. **57**, 205 (2007).
- [31] H. Bichsel, Nucl. Instrum. Meth. A **562**, 154 (2006).
- [32] B. I. Abelev *et al.* [STAR Collaboration], Phys. Rev. C **79**, 034909 (2009).
- [33] M. I. Podgoretsky, Sov. J. Nucl. Phys. **37**, 272 (1983).
- [34] P. Grassberger, Nucl. Phys. B **120**, 231 (1977).
- [35] R. Lednicky and V. L. Lyuboshitz, Sov. J. Nucl. Phys. **35**, 770 (1982).
- [36] M. Gyulassy, S. K. Kauffmann and L. W. Wilson, Phys. Rev. C **20**, 2267 (1979).
- [37] D. H. Boal, C. K. Gelbke and B. K. Jennings, Rev. Mod. Phys. **62**, 553 (1990).
- [38] Yu. Sinyukov, R. Lednicky, S. V. Akkelin, J. Pluta and B. Erazmus, Phys. Lett. B **432**, 248 (1998).
- [39] M. A. Lisa and S. Pratt, arXiv:0811.1352 [nucl-ex].
- [40] P. F. Kolb and U. W. Heinz, arXiv:nucl-th/0305084.
- [41] F. Retiere and M. A. Lisa, Phys. Rev. C **70**, 044907 (2004).
- [42] T. Hirano and K. Tsuda, Nucl. Phys. A **715**, 821 (2003).
- [43] B. Tomasik, U. A. Wiedemann and U. W. Heinz, Nucl. Phys. A **663**, 753 (2000).
- [44] U. A. Wiedemann, P. Scotto and U. W. Heinz, Phys. Rev. C **53**, 918 (1996).
- [45] U. A. Wiedemann, Phys. Rev. C **57**, 266 (1998).
- [46] S. Pratt, Phys. Rev. Lett. **53**, 1219 (1984).
- [47] B. R. Schlei and N. Xu, Phys. Rev. C **54**, R2155 (1996).
- [48] B. R. Schlei, U. Ornik, M. Plumer and R. M. Weiner, Phys. Lett. B **293**, 275 (1992).
- [49] A. N. Makhlin and Y. M. Sinyukov, Z. Phys. C **39**, 69 (1988).
- [50] B. B. Back *et al.* [PHOBOS Collaboration], Phys. Rev. C **73**, 031901 (2006).
- [51] L. Ahle *et al.* [E802 Collaboration], Phys. Rev. C **66**, 054906 (2002).
- [52] D. Adamova *et al.* [CERES Collaboration], Nucl. Phys. A **714**, 124 (2003).
- [53] M. A. Lisa *et al.* [E895 Collaboration], Phys. Rev. Lett. **84**, 2798 (2000).
- [54] I. G. Bearden *et al.* [NA44 Collaboration], Phys. Rev. C **58**, 1656 (1998).
- [55] C. Alt *et al.* [NA49 Collaboration], Phys. Rev. C **77**, 064908 (2008).
- [56] R. A. Soltz *et al.* [E866 Collaboration], Nucl. Phys. A **661**, 439 (1999).
- [57] M. M. Aggarwal *et al.* [WA98 Collaboration], Phys. Rev. C **67**, 014906 (2003).
- [58] Z. W. Lin, C. M. Ko and S. Pal, Phys. Rev. Lett. **89**, 152301 (2002).
- [59] J. G. Cramer, G. A. Miller, J. M. S. Wu and J. H. S. Yoon, Phys. Rev. Lett. **94**, 102302 (2005).
- [60] D. Teaney, Phys. Rev. C **68**, 034913 (2003).
- [61] P. Romatschke, Eur. Phys. J. C **52**, 203 (2007).
- [62] W. Florkowski, W. Broniowski, M. Chojnacki and A. Kisiel, arXiv:0811.3761 [nucl-th].
- [63] S. Pratt, arXiv:0811.3363 [nucl-th].
- [64] W. N. Zhang and C. Y. Wong, arXiv:hep-ph/0702120.
- [65] G. A. Miller and J. G. Cramer, J. Phys. G **34**, 703 (2007).
- [66] D. Adamova *et al.* [CERES Collaboration], Phys. Rev. Lett. **90**, 022301 (2003).
- [67] B. Alessandro *et al.* [ALICE Collaboration], J. Phys. G **32**, 1295 (2006).